



## RESEARCH ARTICLE

# The Biomechanical Effects of Different Bag-Carrying Styles on Lumbar Spine and Paraspinal Muscles: A Combined Musculoskeletal and Finite Element Study

Geng Zhao, MD<sup>1,2#</sup>, Hongwei Wang, PhD<sup>3#</sup>, Lianlei Wang, MD<sup>1#</sup>, Yakubu Ibrahim, MM<sup>2</sup> , Yi Wan, PhD<sup>4</sup>, Junyuan Sun, MD<sup>1,2</sup>, Suomao Yuan, MD<sup>1</sup>, Xinyu Liu, MD<sup>1</sup> 

<sup>1</sup>Department of Orthopedics, Qilu Hospital of Shandong University, <sup>2</sup>Cheeloo College of Medicine and <sup>4</sup>School of Mechanical Engineering, Shandong University and <sup>3</sup>Collage of Artificial Intelligence and Big Data for Medical Sciences, Shandong First Medical University, Jinan, China

**Objectives:** Bags such as handbags, shoulder bags, and backpacks are commonly used. However, it is difficult to assess the biomechanical effects of bag-carrying styles on the lumbar spine and paraspinal muscles using traditional methods. This study aimed to evaluate the biomechanical effects of bag-carrying styles on the lumbar spine.

**Methods:** We developed a hybrid model that combined a finite element (FE) model of the lumbar spine and musculoskeletal models of three bag-carrying styles. The image data was collected from a 26-years-old, 176 cm and 70 kg volunteer. OpenSim and ABAQUS were used to do the musculoskeletal analysis and finite analysis. Paraspinal muscle force, intervertebral compressive force (ICF), and intervertebral shear force (ISF) on L1 were calculated and loaded into the FE model to assess the stress distribution on the lumbar spine.

**Results:** Different paraspinal muscle activation occurred in the three bag-carrying models. The increase in the ICF generated by all three bags was greater than the bags' weights. The handbag produced greater muscle force, ICF, ISF, and peak stress on the nucleus pulposus than the backpack and shoulder bag of the same weight. Peak stress on the intervertebral discs in the backpack model and the L1–L4 segments of the shoulder bag model increased linearly with bag weight, and increased exponentially with bag weight in the handbag model.

**Conclusion:** Unbalanced bag-carrying styles (shoulder bags and handbags) led to greater muscle force, which generated greater ICF, ISF, and peak stress on the lumbar spine. The backpack produced the least burden on the lumbar spine and paraspinal muscles. Heavy handbags should be used carefully in daily life.

**Key words:** Bag-carrying style; Biomechanical effects; Finite element; Lumbar spine; Musculoskeletal model

## Introduction

Bags are typically used for load-carrying and are very convenient in daily life. However, bag-carrying disrupts the normal equilibrium of the human spine.<sup>1</sup> The load on the upper body increases paraspinal muscle stiffness, which is related to the occurrence of low back pain,<sup>2,3</sup> and increases the stress on the nucleus pulposus that indicates high risks of

intervertebral disc degeneration.<sup>4,5</sup> Various kinds of bags, including backpacks, shoulder bags, and handbags, are widely used in daily life.<sup>6</sup> These different kinds of bags have different force action positions and transmission routes on the human body. It is essential to evaluate the biomechanical effects of different bag-carrying styles on the lumbar spine and paraspinal muscles to determine the best bag-carrying

**Address for correspondence** Xinyu Liu, Department of Orthopedics, Qilu Hospital of Shandong University, No.107, Wenhuxi Road, Jinan, Shandong Province, 250012, China. Email: [newyuliu@163.com](mailto:newyuliu@163.com)

<sup>#</sup>Geng Zhao, Hongwei Wang and Lianlei Wang contributed equally to this article.

Received 4 May 2022; accepted 10 October 2022

style to reduce the risk of lumbar disc degeneration and paraspinal muscle injury.

It is difficult to directly measure the biomechanical effects of external load on the lumbar spine using clinical or experimental approaches. Finite element (FE) analysis is a non-invasive method that can comprehensively demonstrate the stress distributions on vertebrae and intervertebral discs under various load or displacement conditions.<sup>7</sup> Conventional FE models of the lumbar spine consist of vertebrae, intervertebral discs, and ligaments,<sup>8</sup> while recently developed models have taken more details into consideration to improve the accuracy of the simulation. Kim *et al.* embedded the annulus fibers in the annulus matrix surrounding the nucleus pulposus.<sup>9</sup> Bojairami *et al.* added the intramuscular pressure, intra-abdominal pressure, and thoracolumbar fascia to a lumbar FE model.<sup>10</sup> However, the structure above the lumbar spine and the load transmission have been ignored, and the load is usually assumed to be a virtual follower load and moment that are applied to the lumbar vertebrae in the FE model.<sup>11</sup> Furthermore, although the FE method has the advantages of evaluating stress and strain on passive structures such as bone, intervertebral discs, and ligaments, the simulation of active muscle contraction is limited.

The musculoskeletal model is a biomechanical model based on inverse kinematics and inverse dynamics that was developed to primarily compute muscle force and joint motion,<sup>12,13</sup> and is capable of calculating the intervertebral reaction force and muscle force. Sturdy *et al.* used a musculoskeletal model to evaluate the axial L4/5 contact force in the backpack and belt-assisted backpack carrying conditions.<sup>14</sup> Actis *et al.* quantified the L4/5 load in people with a transtibial amputation and during sit-to-stand movement.<sup>15</sup> However, the intervertebral joints of musculoskeletal models are assumed to be pivots (frictional or frictionless).<sup>16,17</sup> Therefore, the stress or strain on vertebrae and intervertebral discs cannot be characterized in detail by the musculoskeletal model.

Recently, hybrid models that combine FE and musculoskeletal models have provided a potential method to conduct a comprehensive biomechanical analysis. Khoddam-Khorasani *et al.* developed a hybrid model of the trunk in which the musculoskeletal model estimated the muscle force and the passive FE model predicted the annulus fiber strain.<sup>18</sup> Another hybrid model developed by Liu *et al.* predicted the trunk muscle force and reaction force at the T12/L1 junction in the musculoskeletal model and investigated the effects of intra-abdominal pressure on spinal load-sharing in the FE model.<sup>19</sup> These studies indicated that the hybrid models are valuable in conducting an accurate biomechanical study of the lumbar spine.

Therefore, this study aims to evaluate the biomechanical effects of different bag-carrying styles on the lumbar spine and paraspinal muscles: (1) Paraspinal muscle force was used to evaluate the risk of muscle injury; (2) Intervertebral disc compression force and von Mises stress distribution on intervertebral discs were used to evaluate the risk of intervertebral disc degeneration. The

intervertebral disc compression force and muscle force were simulated by the musculoskeletal model. Furthermore, the force was applied to the FE model of the lumbar spine to evaluate the stress distribution on the vertebrae and intervertebral discs.

## Method

### The Musculoskeletal Model

A musculoskeletal model including the skull, torso, pelvis, upper limbs, and thighs was previously developed in OpenSim (SimTK, Stanford, CA).<sup>20</sup> As shown in Figure 1, the original model represented a 170 cm male subject with 71 kg body weight (BW), and it was scaled to 176 cm to match the volunteer for the FE model. The model included 62 weld joints and 41 custom joints, with six controllable degrees of freedom (DOF) for every lumbar intervertebral joint. The model was consistent with the clinical definition of well-balanced spine, in which the C7 plumb line (C7PL) passed through the posterior superior corner of the sacrum (the value of sagittal vertical axis was 0). The “net passive stiffness” contributed by the intervertebral discs and ligament, and capsules were used at each intervertebral joint to determine its motion.<sup>20</sup> The muscle structure was developed by previous studies.<sup>21–23</sup> Standard OpenSim algorithm which minimized the sum of squared muscle activation was used to calculate the muscle force (Eqn (1)).

$$\sum_{i=1}^n (a_i)^2; \quad (1)$$

$a = \text{muscle activation},$   
 $n = \text{number of muscles}.$

The paraspinal muscles directly connected with the lumbar spine were divided into six groups: psoas major muscle (PS), iliocostalis muscle (IL), quadratus lumborum muscle (QL), latissimus dorsi muscle (LD), longissimus muscle (LG), and multifidus muscle (MF). To study the biomechanical effects of different bag-carrying styles, four models were developed to represent different situations:

1. Unloaded model: original model without any bags.
2. Backpack (BP) model: two backpack-torso joints were defined at two points 10 cm from the midline of the body on the clavicle, which both had three rotational DOF. A force equal to the weight of the backpack was applied equally at two defined points.<sup>14</sup>
3. Shoulder bag (SB) model: one bag-torso joint was defined at the point 10 cm from the midline of the body on the right clavicle, which had three rotational DOF. A force equal to the weight of the shoulder bag was applied at the defined point.
4. Handbag (HB) model: one bag-hand joint was defined at the right waist, which had three rotational DOF. A force equal to the weight of the handbag was applied at the defined point.

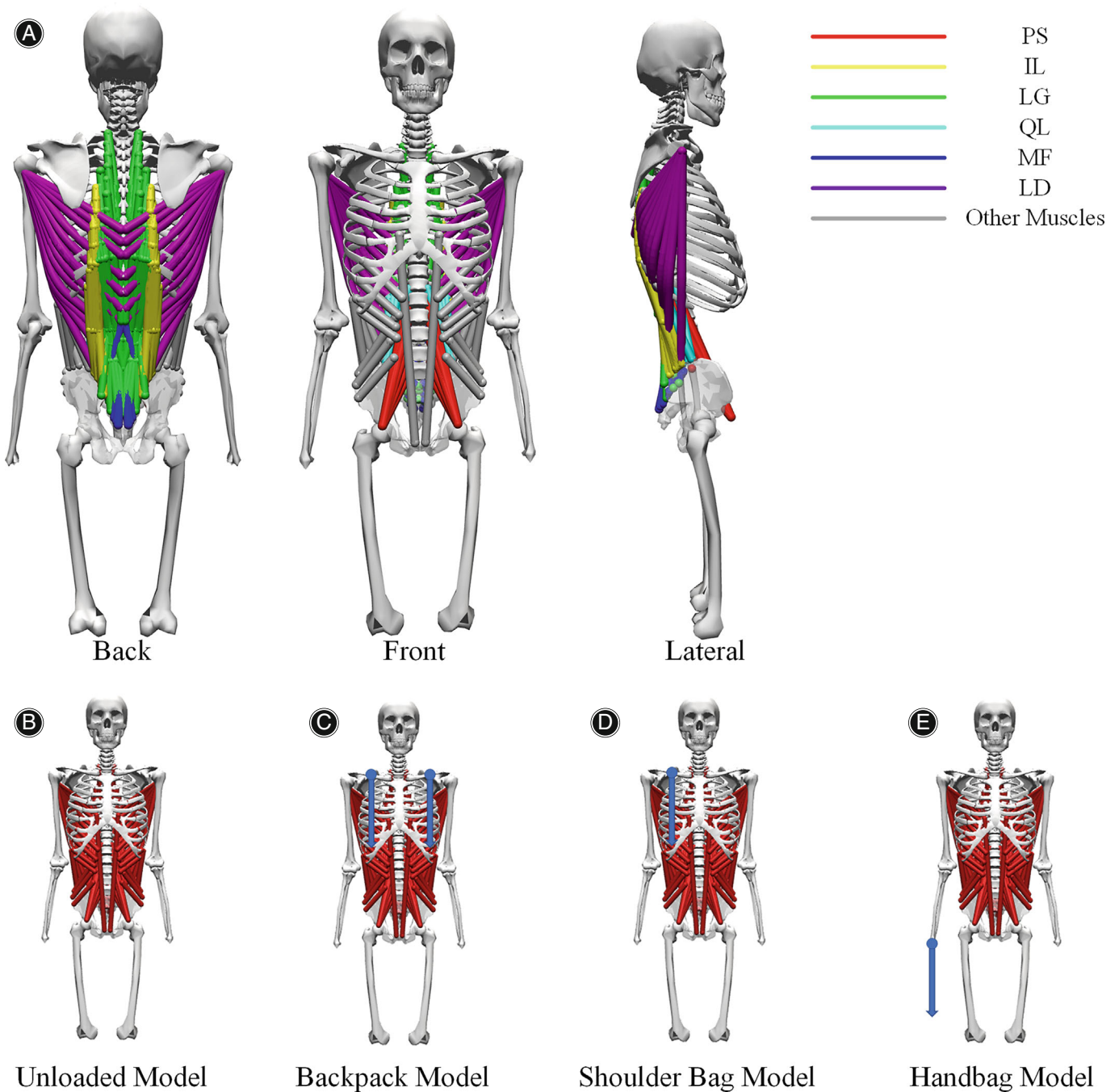


**FIG. 1** Representations of the musculoskeletal models. (A) Posterior, anterior, and lateral views of the musculoskeletal model. (B) The unloaded model. (C) The backpack model. (D) The shoulder bag model. (E) The handbag model

### *The FE Model of Lumbar Spine*

The FE model of lumbar spine was developed based on the CT data of a typical male volunteer (26 years old, 176 cm, and 70 kg) without any spinal disease. The participant provided informed written consent for this study. The CT images of lumbar vertebrae were extracted using Mimics (Materialize NV, Leuven, Belgium), and the intervertebral

discs were established in SolidWorks (SolidWorks Inc., Concord, MA). The model was meshed in HyperMesh (Altair Technologies Inc., Fremont, CA) and calculated in Abaqus/Standard (Simulia Inc., Providence, RI). As shown in Figure 2, the FE model of lumbar spine consisted of cortical bones, cancellous bones, bone endplates, cartilage endplates, annulus matrix, annulus fibers, nucleus, and ligaments. The

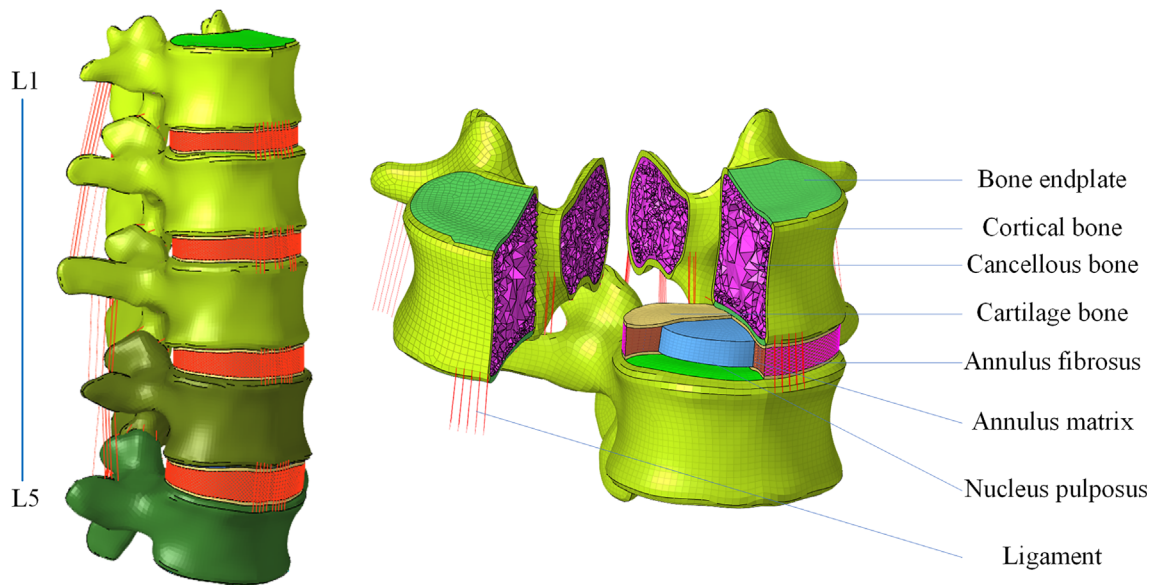


**FIG. 2** Finite element model of the lumbar spine

bone was established as isotropic material. Cortical bone, endplate, annulus matrix, and nucleus were meshed using hexahedral elements, while cancellous bone was meshed using tetrahedral elements.<sup>24,25</sup> The thickness of cortical bone was assumed as 1 mm.<sup>26</sup> The facet joints were defined as frictionless contact.<sup>27</sup> Annular fibers, which were added into the annulus matrix, were meshed as nonlinear truss elements with no compression. The annulus fibers were aligned with the angle from 30° to 45° in a crisscross pattern.<sup>28</sup> The inferior endplate of L5 were restricted in six DOFs. The attachment area of paraspinal muscles was defined based on the study of anatomy.<sup>29–35</sup> The global element size of 1 mm was used to mesh the FE model. In total, 306,448 nodes and 1,022,787 elements were used in the model. All the material properties are assumed based on previous studies,<sup>36–38</sup> which were shown in Table 1.

### Validation

To validate the musculoskeletal model, the intervertebral compressive force (ICF) of the musculoskeletal model from neutral position to 45° flexion was compared to that of previous studies.<sup>39–42</sup> In the FE model, the inferior endplate of L5 was fixed and a 400 N compression force and a 10 Nm moment were applied on the superior endplate of L1 to mimic the physiological motions of extension, flexion, bending, and torsion. Muscle force in the musculoskeletal model was also compared with that in the electromyography-driven (EMGD) and kinematics-driven (KD) model from Arjmand *et al.*<sup>43</sup> The ranges of motion (ROM) in the previous experimental and FE studies were taken as references to validate the FE model.<sup>44–48</sup>

### Simulation Workflow

The direction of paraspinal muscles was determined by the coordinates of the origins and terminations in the musculoskeletal model, and then it was applied to the FE model. To assess the biomechanical effects of different bag-carrying styles and bag weights on lumbar spine and paraspinal muscles, the forces used to simulate the different bags were assumed equal to the 5%, 10%, 15%, and 20% BW and were added to the BP, SB, and HB models,<sup>6,49</sup> and no external load was added to the UL model. In the musculoskeletal model, the paraspinal muscle force, ICF, and intervertebral shear force (ISF) from T12/L1 to L5/S1 in neutral standing posture were calculated. Furthermore, six groups of tension were added on each vertebra to represent muscle force according to the attachment points and directions of paraspinal muscles in anatomy. In all models, the ICF and ISF on the T12/L1 disc was applied to the L1 superior endplate and the muscle force was applied to the six muscle groups in the FE model of lumbar spine to calculate the von mises stress on the lumbar spine (Figure 3).

## Results

### Validation

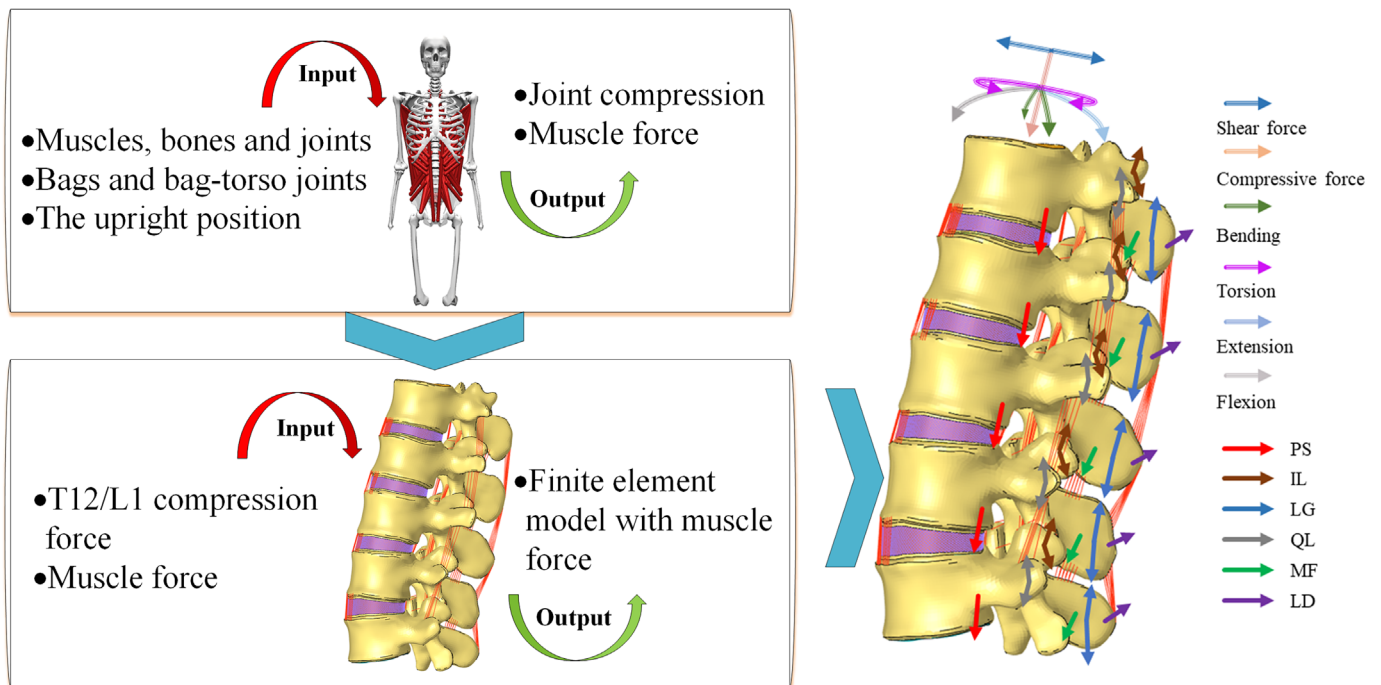
As shown in Figure 4, the results of comparison revealed a good agreement between the musculoskeletal model and the experimental data.<sup>39–42</sup> In previous studies, the ICF of L3/4 in the neutral upright position was 441N,<sup>39</sup> the ICF of the lower segment was 82%BW,<sup>40</sup> the ICF of L4/5 at 36° flexion increased to 116% of it in neutral position,<sup>41</sup> the ICF at 45° flexion of L1/2 increased to 124% of it in neutral position,<sup>42</sup> and the ICF at 19° extension of L4/5 increased to 129% of it



**TABLE 1** Material properties of the developed FE model

Component	Young's modulus (MPa)	Poisson's ratio	Cross-section area (mm <sup>2</sup> )
Cortical bone	12,000	0.3	-
Cancellous bone	100	0.2	-
Bone endplate	12,000	0.3	-
Cartilage endplate	25	0.25	-
Annulus matrix	4.2	0.45	-
Nucleus pulposus	1	0.4999	-
Anterior longitudinal ligament	7.8	0.3	63.7
Posterior longitudinal ligament	10	0.3	14.4
Capsular ligament	7.5	0.3	30
Ligamentum flavum	15	0.3	40
Interspinous ligament	10	0.3	26
Supraspinal ligament	8	0.3	23
Transverse ligament	10	0.3	1.8
AF layer 1	550	0.3	0.7
AF layer 2	495	0.3	0.63
AF layer 3	440	0.3	0.55
AF layer 4	420	0.3	0.49
AF layer 5	385	0.3	0.41
AF layer 6	360	0.3	0.3

Abbreviation: AF, annulus fibers.

**FIG. 3** Workflow from the musculoskeletal model to the finite element model

in neutral position.<sup>41</sup> In this musculoskeletal model, the ICF of L3/4 in the neutral upright position was 446 N, which was 110.2% of the reference. The ICF of L4/5 was 580 N, 81.7% BW, which was 99.7% of the reference. The ICF of L4/5 at 36° flexion increased to 120% of it in neutral position, which was 103% of the reference. The ICF of L1/2 at 45° flexion

increased to 210% of it in neutral position, which was 94.1% of the reference. And the ICF of L4/5 at 19° extension increased to 128% of it in neutral position, which was 99.2% of the reference. Muscle force in this musculoskeletal model also has good consistency with that in the EMGD model and KD model. In the FE model, under flexion, extension,

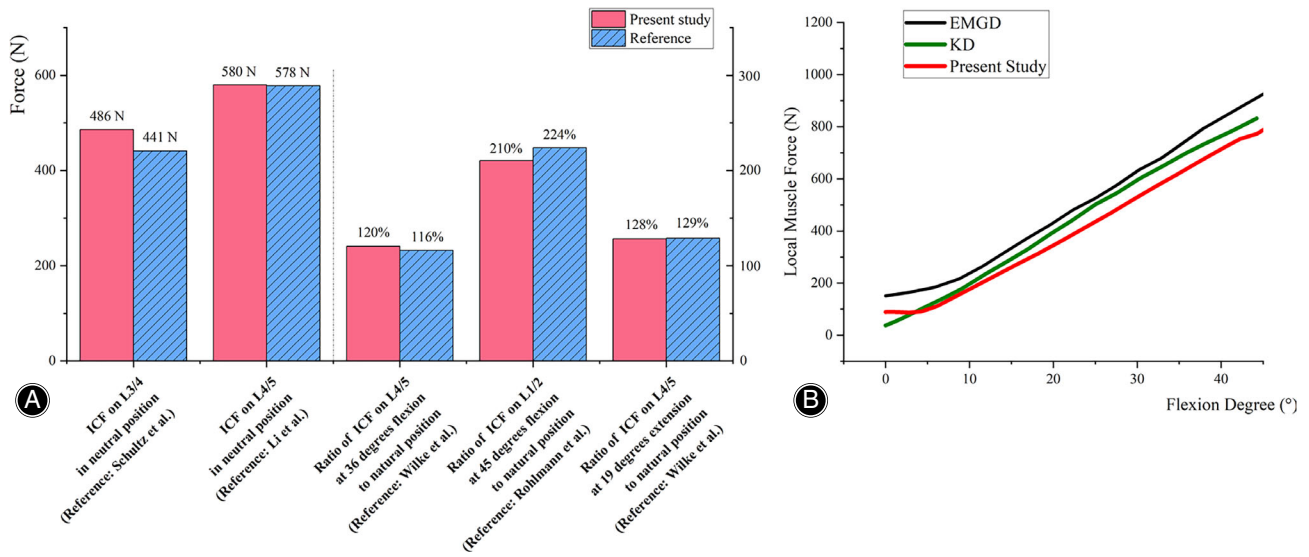


**FIG. 4** Validation of the musculoskeletal model. (A) Comparison of the intervertebral compressive force (ICF) predicted in this musculoskeletal model with it in previous studies during standing-flexion motion. (B) Comparison of local muscle force (IL, iliocostalis muscle; LG, longissimus muscle; MF, multifidus muscle; and QL, quadratus lumborum muscle) predicted in this musculoskeletal model with it in the electromyography-driven (EMGD) and kinematics-driven (KD) model from Arjmand *et al.*

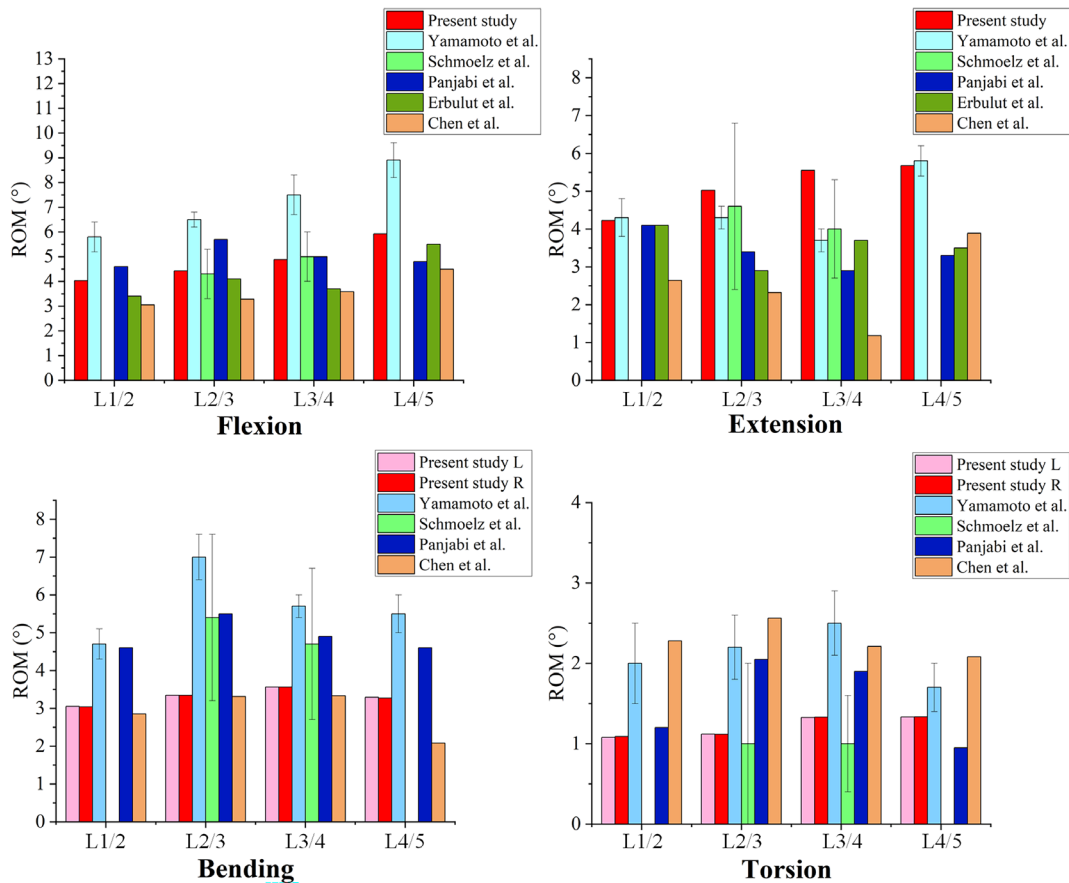


**FIG. 5** Validation of the finite element model by comparing the ROMs with the previous studies. ROM, range of motion

bending, and torsion load conditions, the ROMs of each segment were compared with the previous studies and showed satisfactory agreements (Figure 5). Therefore, the FE model of lumbar spine was effective to assess the biomechanical effect of bags on lumbar spine.

### Muscle Force

As shown in Figure 6, paraspinal muscle force in neutral position increased with bag weight increasing in all bag-carrying models. The paraspinal muscle force in the HB model increased most while in the BP model it increased the

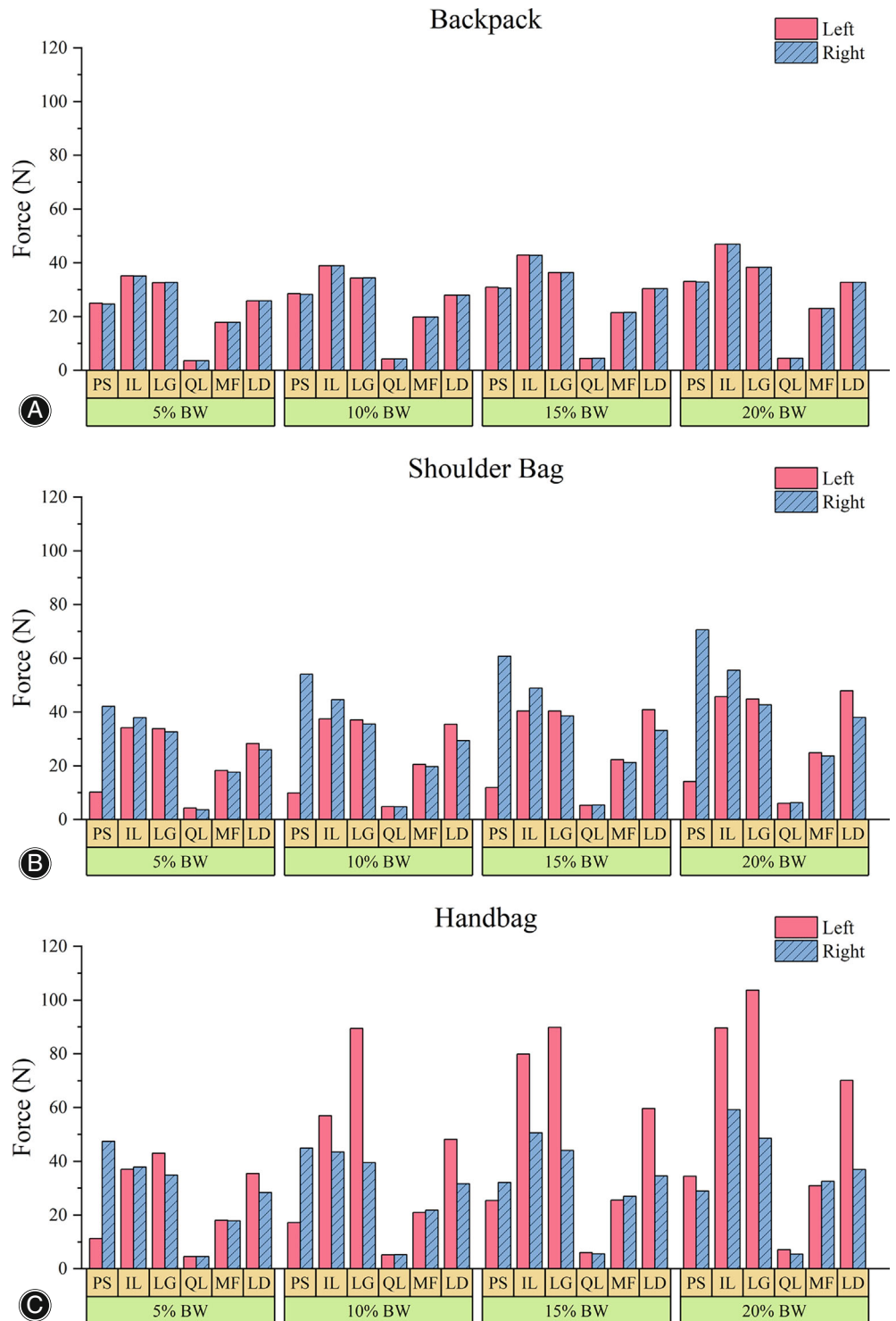


**FIG. 6** Paraspinal muscle force with the increase in bag weight (as a percentage of body weight (BW)) in the (A) backpack model, (B) shoulder bag model, and (C) handbag model. The assessed muscles were the psoas major muscle (PS), iliocostalis muscle (IL), quadratus lumborum muscle (QL), latissimus dorsi muscle (LD), longissimus muscle (LG), and multifidus muscle (MF)

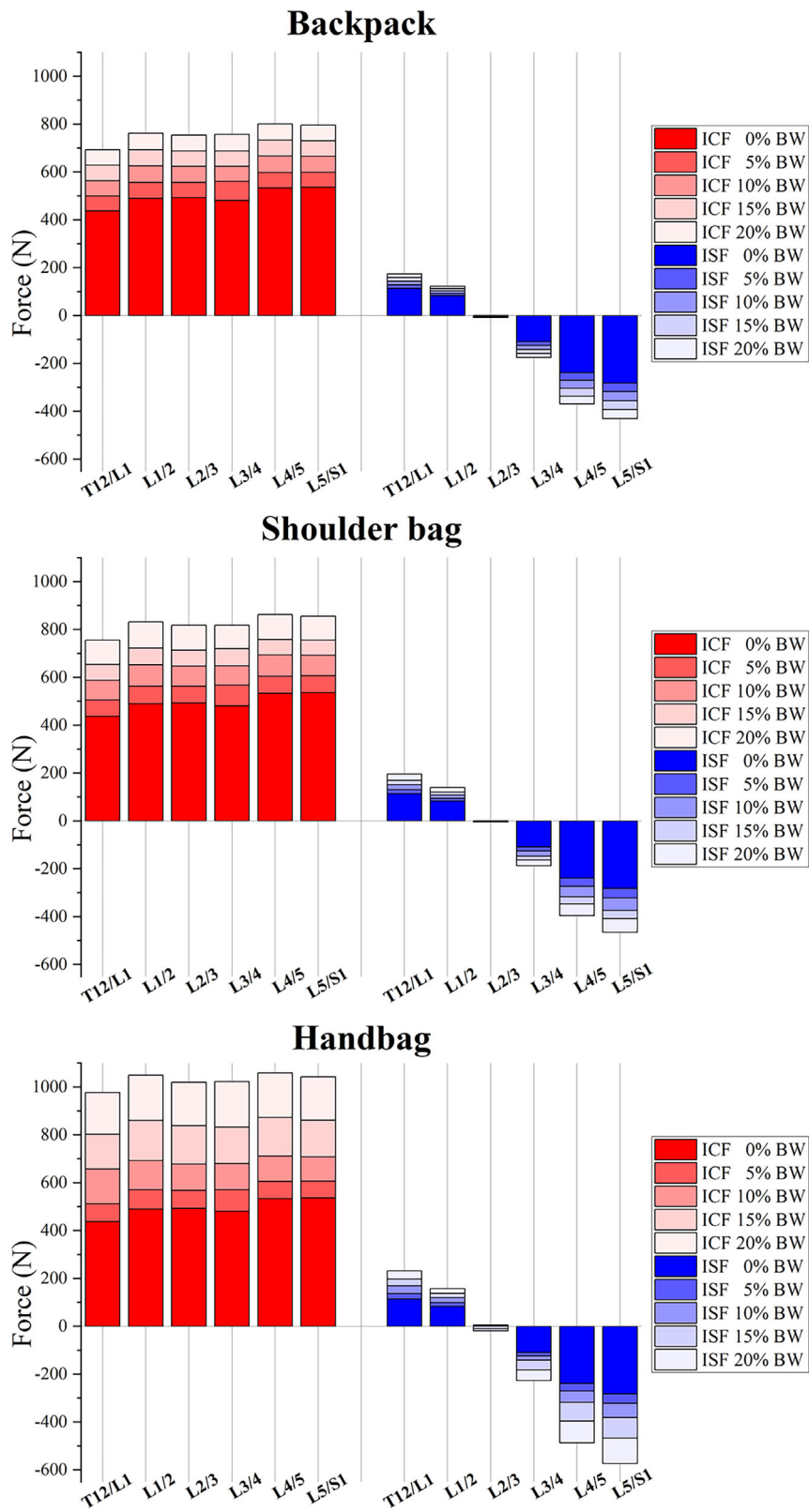


**FIG. 7** ICF and ISF in the three bag-carrying models. The positive values of ISF meant that the direction of force was posterior, and the negative values of ISF meant that the direction was anterior. ICF, intervertebral compressive force; ISF, intervertebral shear force



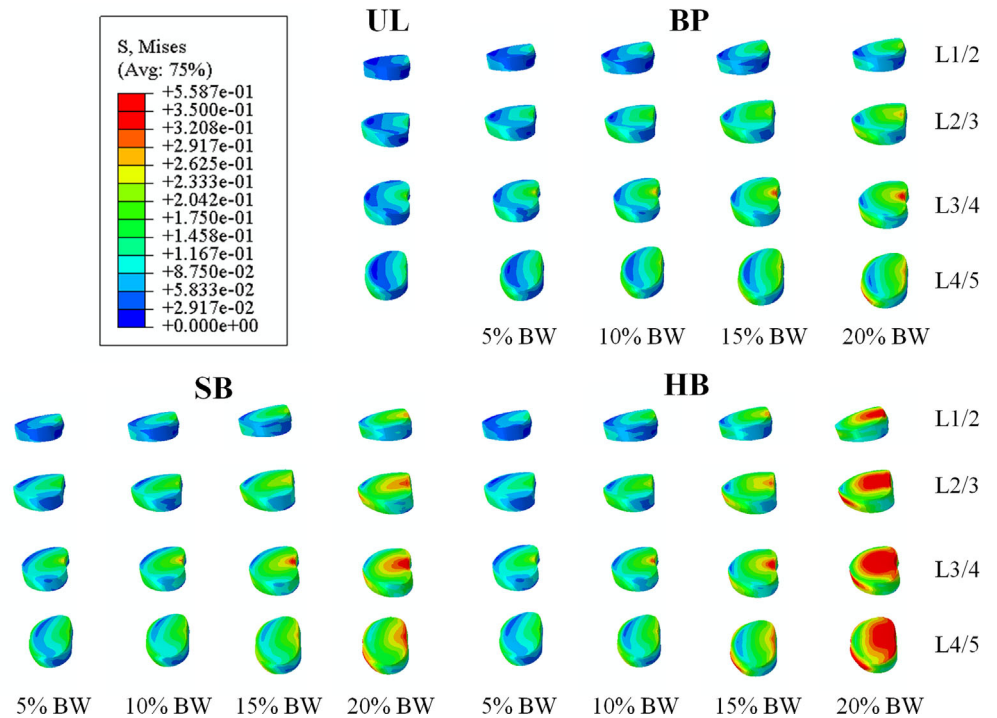


**FIG. 8** Stress distribution on the nucleus pulposus in the backpack (BP) model, shoulder bag (SB) model, and handbag (HB) model

least. The paraspinal muscle force in the BP model was balanced on the left and right sides. In the SB model, muscle force of PS and IL on the right side was higher than that on the left side, and muscle force of LG, MF, and LD on the left side was higher. In the HB model, muscle force of IL, LG, and LD on the left side was higher than that on the right side, and muscle force of MF was slightly higher on the right side. The value of muscle force of PS on the left side exceeded that on the right when the handbag weighed 20% BW.

#### Intervertebral Disc Force

The ICF and ISF of lumbar spine were shown in Figure 7. The ICF increased from T12/L1 to L1/2, varied slightly from L1/2 to L3/4 and then reached the peak at L4/5 and L5/S1 segments. As the bag weight increased from 0% to 20% BW, the ICF of T12/L1 in the BP, SB, and HB models increased by 255 N, 317 N and 539 N, respectively. The ISF decreased from T12/L1 to L2/3 and changed the direction from posterior to anterior at L3/4 in all models. The ISF value on L2/3 was approximately zero. The greatest ISF occurred at L5/S1 (148 N, 183 N and 291 N in BP, SB and HB models with 20% BW bag, respectively). As the bag weight increased from 0% to 20% BW, the ISF at T12/L1 in the BP, SB, and HB models increased by 61 N, 83 N, and 118 N, respectively.

#### Von Mises Stress on the Nucleus Pulposus

As shown in Figure 8, the stress on the nucleus pulposus increased from the proximal segments to the distal segments in the three bag-carrying models, and was concentrated in the posterior part of the nucleus pulposus. In addition, the

peak stress on the nucleus pulposus increased with bag weight increasing. Compared with the UL model, the peak stress on the nucleus pulposus in BP, SB, and HB models with bags of 5% BW increased by 8.2%, 13.9%, and 16.1%, respectively. The peak stress in BP, SB, and HB models with bags of 10% BW increased by 25.0%, 34.7%, and 46.5%, respectively. The peak stress in BP, SB, HB models with bags of 15% BW increased by 44.5%, 60.0%, and 84.6%, respectively. The peak stress in BP, SB, and HB models with bags of 20% BW increased by 64.6%, 98.8%, and 164.7%, respectively. The increase of peak stress in the HB model was higher than that in the SB and HB models.

#### Von Mises Stress on the Vertebrae

Due to the attachment of muscles and the shape of vertebral body, the stress was concentrated in the anterior edge of the vertebrae and the pars interarticularis in the three bag-carrying models (Figure 9). Furthermore, the stress on the vertebrae increased from the proximal segments to the distal segments in the three bag-carrying models. The stress on the same vertebrae in the HB model was the highest in the three bag-carrying styles, which was followed by that in the SB model.

#### Discussion

This study combined the musculoskeletal model and the FE model of lumbar spine to investigate the biomechanical effects of different bag-carrying styles. The paraspinal muscle force, ICF, and ISF on each intervertebral disc were determined for each individual model and the stress

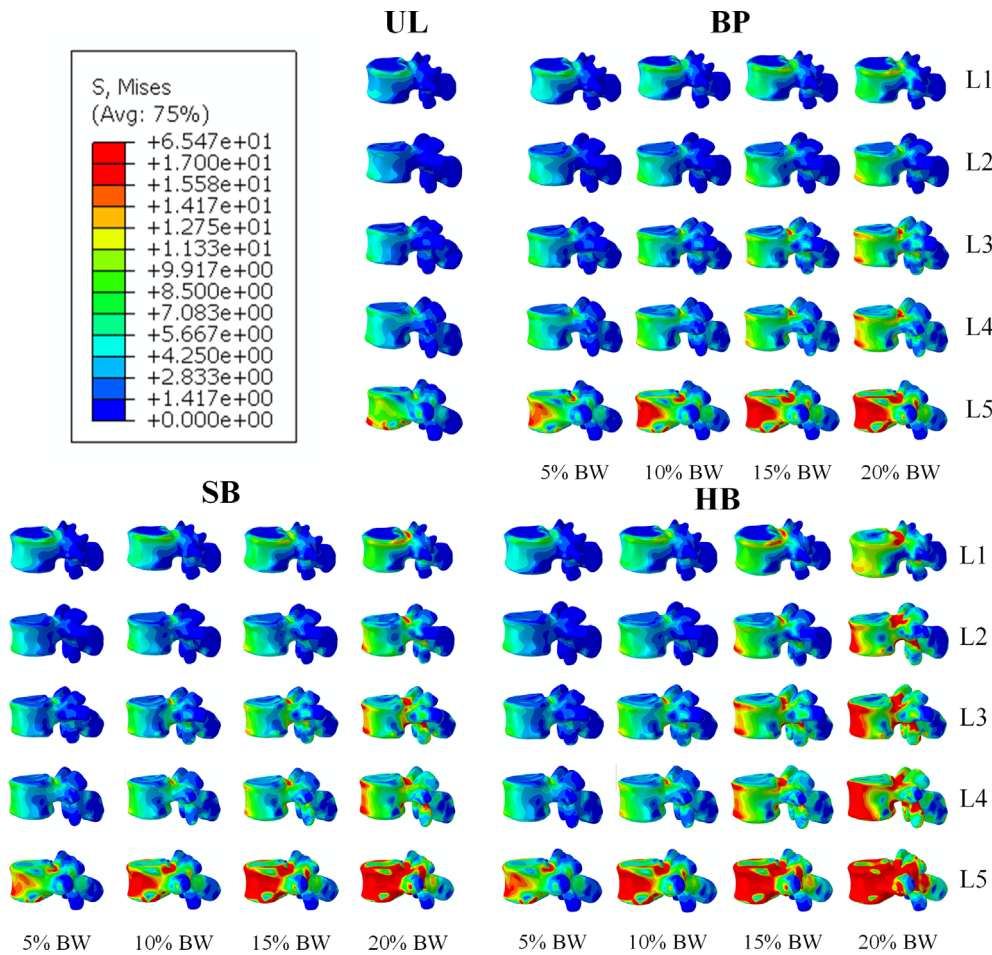


**FIG. 9** Stress distribution on the vertebrae in the backpack (BP) model, shoulder bag (SB) model, and handbag (HB) model

TABLE 2 Regression equations of the peak stress values on the nucleus pulposus with bag weight			
Segment	Backpack	Shoulder bag	Handbag
L1-L2	$y = 0.118 + 0.008x$ $R^2 = 0.9924$	$y = 0.112 + 0.012x$ $R^2 = 0.9720$	$y = 0.058 + 0.064e0.119x$ $R^2 = 0.9994$
L2-L3	$y = 0.146 + 0.009x$ $R^2 = 0.9686$	$y = 0.142 + 0.012x$ $R^2 = 0.9683$	$y = 0.096 + 0.059e0.121x$ $R^2 = 0.9990$
L3-L4	$y = 0.978 + 0.010x$ $R^2 = 0.9937$	$y = 0.221 + 0.013x$ $R^2 = 0.9780$	$y = 0.189 + 0.046e0.146x$ $R^2 = 0.9965$
L4-L5	$y = 0.213 + 0.008x$ $R^2 = 0.9681$	$y = 0.191 + 0.035e0.131x$ $R^2 = 0.9964$	$y = 0.212 + 0.018e0.209x$ $R^2 = 0.9969$

distribution on nucleus pulposus and vertebrae was calculated respectively. Although it was well-known that carrying a handbag is more tiring than carrying a backpack, this study combining the musculoskeletal model and FE model of lumbar explained how bag-carrying styles influenced the lumbar spine.

**Muscle Force**

Muscle activation and contraction were important factors in maintaining trunk stiffness in all potential instability activities. Due to the complexity of coordination between

paraspinal muscles, the strategies of muscle activation varied in the three bag-carrying styles. The BP model showed the best balance of muscle force in the left and right sides. The deviation of load position from the midline would lead to a trend of imbalance, and muscles were active to maintain the body in neutral position. In the SB model, PS on the loaded side provided the most force of contraction. In the HB model, the paraspinal muscles on the unloaded side provided more contraction force totally, and the muscle force of IL, LG, and LD increased most rapidly with the bag weight increasing. The muscle activation strategies were different

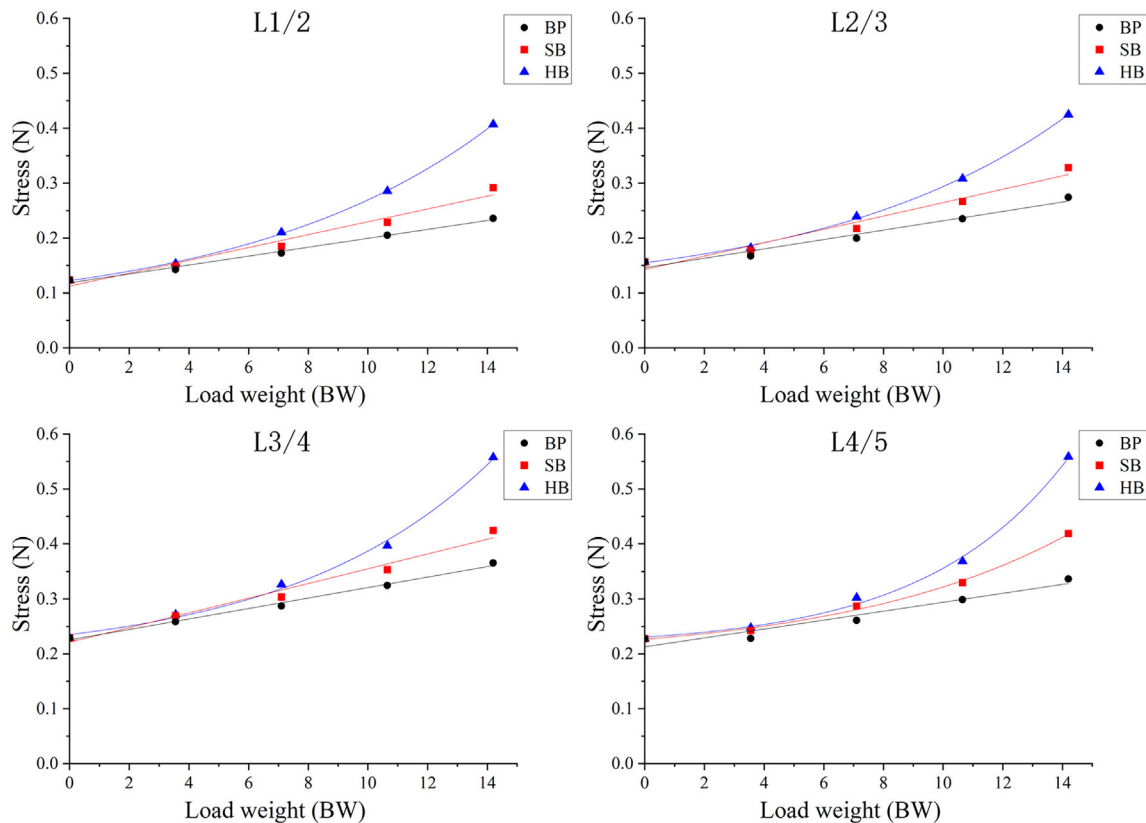


FIG. 10 Regression analysis of peak stress values on the nucleus pulposus with load weight

among the three load-carrying styles. As a result of the asymmetric muscle activation, changing the load side of the shoulder bag or handbag during bag-carrying activities would protect muscles from continuous high tension, which would decrease the risk of muscle injury. In addition to the paraspinal muscles, other muscles, which did not directly connect to the lumbar spine, coordinate with the paraspinal muscles to maintain the balance of body.<sup>50</sup> More evaluation of muscles around the trunk might further assist the analysis of the biomechanical effect of different bag-carrying styles on the human body.

#### Intervertebral Disc Compression Force

Bag-carrying styles also influenced the intervertebral disc force. The values of ICF and ISF in the HB model were higher than that in the BP and SB models with the same bag weight. Paraspinal muscles were activated to maintain postural stability, but the muscle force also induced the increase of lumbar ICF and ISF. The increase of lumbar ICF values was higher than the bag weight in the three bag-carrying styles and was most significantly in the HB model. In our study, the value of ISF was approximately zero at L2/3 segment and increased along the spine in two directions, reaching peak at L5/S1. This showed that the L2/3 was closest to the inflection point of ISF in this model. As the lumbar lordosis varied from individual, the inflection points of ISF showed differences. Liu et al.<sup>19</sup>

reported that the shear force changed directions at L4/5 segment in neutral standing position and reached peak at L1/2. Wettenschwiler *et al.*<sup>51</sup> reported that L2/3 was the inflection point of ISF, and found that the lumbar curvature and keep the ICF the same in any lumbar segment.

#### Von Mises Stress Distribution on the Nucleus Pulposus

Excessive stress on nucleus pulposus was a causative factor of lumbar disc degeneration or herniation, as indicated by the previous study.<sup>42,52,53</sup> The nucleus pulposus, located in the center of the intervertebral disc, was surrounded by the annulus fibrosus. This study demonstrated that the stress concentrated in the posterior part of the nucleus pulposus, which revealed that bag-carrying might increase the risk of lumbar disc posteriorly herniating. The peak stress on the L3/4 and L4/5 segments was higher than that on the L1/2 and L2/3 segments, which was consistent with more clinical diseases occurring at low segments.<sup>54</sup>

With bag weight increasing, the increase rate of the stress on the nucleus pulposus in the three bag-carrying styles were different. To validate the trend of peak stress increasing, the peak stress values on the nucleus pulposus was compared with bag weight by linear regression (12 regression equations in total). The *p*-values of seven linear regression equations (L1/2, L2/3, L3/4, L4/5 in BP model

and L1/2, L2/3, L3/4 in SB model) were less than 0.01, which meant that these linear regression equations had high statistical significance. But the  $p$ -values in the other five linear regression equations (L4/5 in SB model and L1/2, L2/3, L3/4, L4/5 in BP model) were higher than 0.01. Then, exponential regression analysis was tried on the latter segments, and the  $p$ -values of the exponential regression were less than 0.01, which meant that these exponential regression equations had high statistical significance. The regression equations and correlation coefficients are displayed in Table 2 and Figure 10.  $R^2$  (correlation coefficient) in the 12 regression equations were all higher than 0.95, indicating that the regression equations had high fitting degrees. The regression analysis showed that there was a linear correlation between peak stress on nucleus pulposus and bag weight at all segments of BP model and L1–4 segments of SB model, and there was an exponential correlation between peak stress on nucleus pulposus and bag weight at all segments of HB model and L4/5 segment of SB model. When the bag weighed less than 15% BW, the stress on nucleus pulposus were not much different among the three bag-carrying styles. However, when the bag weight exceeded 15% BW, the stress increased rapidly in the HB model.

Even though there are different values of ICF and stress on nucleus pulposus, the stress distribution on nucleus pulposus was evenly distributed on the left and right side in the three bag-carrying models, which was the result of muscle activation. It meant that bag-carrying styles affected the paraspinal muscle force, ICF, and ISF, but the position of peak stress on nucleus pulposus remained on the posterior part in the standing posture. Changing the load side could relieve the tension of paraspinal muscle but not reduce the burden of intervertebral discs.

Hong *et al.* reported that a bag of 15% BW or above significantly increased the muscle force and was deleterious to the musculoskeletal system in children.<sup>6</sup> Wettenschwiler *et al.* suggested that the backpack weighting 40 kg or more might increase the risk of lumbar injuries unless more load was transferred to the hips.<sup>51</sup> The present study researched the different biomechanical effects of the backpack, shoulder bag, and handbag. When the bag weight was less than 10% BW, there were no significant differences of the biomechanical effects on lumbar spine among three bag-carrying styles. However, when the bag weight exceeded 15% BW, the handbag led to significantly high burden of paraspinal muscles and intervertebral discs. For those who use heavy bags every day, reducing the using of handbags can decrease risks for lumbar intervertebral disc degeneration and herniation.

### Strengths and Limitations

In summary, this study compared the muscle force, intervertebral disc compression force and stress distribution on lumbar spine among three kinds of bag-carrying styles using the

musculoskeletal model and lumbar finite element model. This study demonstrated the different biomechanical effects on lumbar spine with different bag-carrying styles. It also provided a method for assessing the biomechanical effects of external loads on the internal bones and muscles of the human body.

There were several limitations in our study. The models used in this study were developed from a male volunteer. Due to the physiological differences, there might be a deviation in the conclusion for women. Only the neutral standing position was simulated by musculoskeletal model. But there are complex activities such as walking in our daily life, and the strain rate also effects the mechanical behavior of the intervertebral discs.<sup>55</sup> Future works are needed to analyze the biomechanical effects of more activities.

### Conclusion

The present study combined the musculoskeletal model and FE model to analyze the biomechanical effects of different bag-carrying styles on lumbar spine. All bags would lead to more ICF on lumbar intervertebral discs than the bag weight, especially when using a handbag. Peak stress on intervertebral discs in all segments of the BP model and L1–4 segments of the SB model increased linearly with bag weight, while it increased exponentially with bag weight in the HB model. The handbag produced higher paraspinal muscle force, ICF, ISF, and peak stress on nucleus pulposus than the backpack and shoulder bag, which would lead to a higher risk of lumbar disc degeneration. As the peak stress increased rapidly, heavy handbags should be used carefully in daily life.

### Acknowledgment

This article is supported by the National Natural Science Foundation of China (Grant No. 81874022).

### Conflict of Interest

All authors declare that they have no conflict of interest.

### Authorship Declaration

All authors listed meet the authorship criteria according to the latest guidelines of the International Committee of Medical Journal Editors, and all authors are in agreement with the manuscript.

### Author Contribution

Genq Zhao: software, writing—original draft; Hongwei Wang: software, validation; Lianlei Wang: writing - review & editing, investigation; Yakubu Ibrahim: writing—review & editing; Yi Wan: resources, supervision; Junyuan Sun: formal analysis; Suomao Yuan: supervision; Xinyu Liu: writing—review & editing, project administration, funding acquisition.

### References

1. Hough PA, Nel M, Smit JE, Malan E, Van Der Watt M, Deacon AF, et al. The influence of carrying a school bag on the developing spine. *Child Health Care*. 2006;35:339–48.

2. Jeon C, Yoo K. The effects of various bag-carrying styles on the muscle tone and stiffness and the spinal alignment of adults with rounded shoulder posture during treadmill walking. *J Int Acad Phys Ther Res*. 2019;10:1840–8.



3. Chaffin DB, Ashton-Miller JA. Biomechanical aspects of low-Back pain in the older worker. *Exp Aging Res.* 1991;17:177–87.
4. Adams MA, Roughley PJ. What is intervertebral disc degeneration, and what causes it? *Spine.* 2006;31:2151–61.
5. Hashimoto K, Aizawa T, Kanno H, Itoi E. Adjacent segment degeneration after fusion spinal surgery—a systematic review. *Int Orthop.* 2019;43:987–93.
6. Hong Y, Li JX. Influence of load and carrying methods on gait phase and ground reactions in children's stair walking. *Gait Posture.* 2005;22:63–8.
7. Dreischarf M, Zander T, Shirazi-Adl A, Puttlitz CM, Adam CJ, Chen CS, et al. Comparison of eight published static finite element models of the intact lumbar spine: predictive power of models improves when combined together. *J Biomech.* 2014;47:1757–66.
8. Goel VK, Clausen JD. Prediction of load sharing among spinal components of a C5-C6 motion segment using the finite element approach. *Spine.* 1998;23:684–91.
9. Kim HJ, Chun HJ, Lee HM, Kang KT, Lee CK, Chang BS, et al. The biomechanical influence of the facet joint orientation and the facet tropism in the lumbar spine. *Spine J.* 2013;13:1301–8.
10. El Bojairami I, Driscoll M. Coordination between trunk muscles, thoracolumbar fascia, and intra-abdominal pressure toward static spine stability. *Spine.* 2021;47:E423–31. <https://doi.org/10.1097/brs.0000000000004223>
11. Joukar A, Kiapour A, Shah A, Vosoughi AS, Goel VK. Sacroiliac joint stabilization using implants provide better fixation in females compared to males: a finite element analysis. *Eur Spine J.* 2021;30:2351–9.
12. Phillips ATM, Villette CC, Modenese L. Femoral bone mesoscale structural architecture prediction using musculoskeletal and finite element modelling. *Int Biomech.* 2015;2:43–61.
13. Yoder AJ, Petrella AJ, Silverman AK. Trunk-pelvis motion, joint loads, and muscle forces during walking with a transtibial amputation. *Gait Posture.* 2015; 41:757–62.
14. Sturdy JT, Sessoms PH, Silverman AK. A backpack load sharing model to evaluate lumbar and hip joint contact forces during shoulder borne and hip belt assisted load carriage. *Appl Ergon.* 2021;90:103277.
15. Actis JA, Nolasco LA, Gates DH, Silverman AK. Lumbar loads and trunk kinematics in people with a transtibial amputation during sit-to-stand. *J Biomech.* 2018;69:1–9.
16. Cholewicki J, McGill SM. Mechanical stability of the in vivo lumbar spine: implications for injury and chronic low back pain. *Clin Biomech.* 1996;11:1–15.
17. Hajihosseinali M, Arjmand N, Shirazi-Adl A, Farahmand F, Ghiasi MS. A novel stability and kinematics-driven trunk biomechanical model to estimate muscle and spinal forces. *Med Eng Phys.* 2014;36:1296–304.
18. Khoddam-Khorasani P, Arjmand N, Shirazi-Adl A. Trunk hybrid passive-active musculoskeletal modeling to determine the detailed T12-S1 response under in vivo loads. *Ann Biomed Eng.* 2018;46(11):1830–43.
19. Liu T, Khalaf K, Naserkhaki S, El-Rich M. Load-sharing in the lumbosacral spine in neutral standing & flexed postures – a combined finite element and inverse static study. *J Biomech.* 2018;70:43–50.
20. Senteler M, Weisse B, Rothenfluh DA, Snedeker JG. Intervertebral reaction force prediction using an enhanced assembly of OpenSim models. *Comput Methods Biomech Biomed Eng.* 2016;19:538–48.
21. Christophy M, Faruk Senan NA, Lotz JC, O'Reilly OM. A musculoskeletal model for the lumbar spine. *Biomech Model Mechanobiol.* 2012 Jan;11(1–2): 19–34.
22. Vasavada AN, Brault JR, Siegmund GP. Musculotendon and fascicle strains in anterior and posterior neck muscles during whiplash injury. *Spine.* 2007;32(7):756–65.
23. Holzbaur KR, Murray WM, Delp SL. A model of the upper extremity for simulating musculoskeletal surgery and analyzing neuromuscular control. *Ann Biomed Eng.* 2005;33(6):829–40.
24. Guo LX, Wang ZW, Zhang YM, Lee KK, Teo EC, Li H, et al. Material property sensitivity analysis on resonant frequency characteristics of the human spine. *J Appl Biomech.* 2009;25:64–72.
25. Wu Y, Wang Y, Wu J, Guan J, Mao N, Lu C, et al. Study of double-level degeneration of lower lumbar spines by finite element model. *World Neurosurg.* 2016;86:294–9.
26. Wang H, Wan Y, Liu X, Ren B, Xia Y, Liu Z. The biomechanical effects of Ti versus PEEK used in the PLIF surgery on lumbar spine: a finite element analysis. *Comput Methods Biomech Biomed Eng.* 2020;0:1–10.
27. Hsieh YY, Chen CH, Tsuang FY, Wu LC, Lin SC, Chiang CJ. Removal of fixation construct could mitigate adjacent segment stress after lumbosacral fusion: a finite element analysis. *Clin Biomech.* 2017;43:115–20.
28. Bashkuev M, Reitmaier S, Schmidt H. Effect of disc degeneration on the mechanical behavior of the human lumbar spine: a probabilistic finite element study. *Spine J.* 2018;18(10):1910–20.
29. Bogduk N, Macintosh JE, Percy MJ. A universal model of the lumbar back muscles in the upright position. *Spine.* 1992 Aug;17(8):897–913.
30. Bogduk N, Percy MJ, Hadfield G. Anatomy and biomechanics of psoas major. *Clin Biomech.* 1992;7(2):109–19.
31. Santaguida P, McGill S. The psoas major muscle: a three-dimensional geometric study. *J Biomech.* 1995;28(3):339–45.
32. Macintosh JE, Bogduk N. The biomechanics of the lumbar multifidus. *Clin Biomech.* 1986;1:205–13.
33. Phillips S, Mercer S, Bogduk N. Anatomy and biomechanics of quadratus lumborum. *Proc. Inst. Mech. Eng., Part H.* 2008;222(2):151–9.
34. Macintosh JE, Bogduk N. Volvo award in basic science. The morphology of the lumbar erector spinae. *Spine.* 1987;12(7):658–68.
35. Bogduk N, Johnson G, Spalding D. The morphology and biomechanics of latissimus dorsi. *Clin Biomech.* 1998;13(6):377–85.
36. Denozière G, Ku DN. Biomechanical comparison between fusion of two vertebrae and implantation of an artificial intervertebral disc. *J Biomech.* 2006; 39:766–75.
37. Kim HJ, Kang KT, Chun HJ, Lee CK, Chang BS, Yeom JS. The influence of intrinsic disc degeneration of the adjacent segments on its stress distribution after one-level lumbar fusion. *Eur Spine J.* 2015;24:827–37.
38. Kang KT, Koh YG, Son J, Yeom JS, Park JH, Kim HJ. Biomechanical evaluation of pedicle screw fixation system in spinal adjacent levels using polyetheretherketone, carbon-fiber-reinforced polyetheretherketone, and traditional titanium as rod materials. *Compos. Part B.* 2017;130:248–56.
39. Schultz A, Andersson G, Ortengren R, Haderspeck K, Nachemson A. Loads on the lumbar spine. Validation of a biomechanical analysis by measurements of intradiscal pressures and myoelectric signals. *J Bone Jt Surg Am.* 1982;64: 713–20.
40. Li SSW, Chow DHK. Effects of backpack load on critical changes of trunk muscle activation and lumbar spine loading during walking. *Ergonomics.* 2018; 61:553–65.
41. Wilke HJ, Neef P, Hinze B, Seidel H, Claes L. Intradiscal pressure together with anthropometric data—a data set for the validation of models. *Clin Biomech.* 2001;16:S111–26.
42. Rohmann A, Graichen F, Kayser R, Bender A, Bergmann G. Loads on a telemeterized vertebral body replacement measured in two patients. *Spine.* 2008; 33:1170–9.
43. Arjmand N, Gagnon D, Plamondon A, Shirazi-Adl A, Larivière C. A comparative study of two trunk biomechanical models under symmetric and asymmetric loadings. *J Biomech.* 2010;43(3):485–91.
44. Yamamoto I, Panjabi M, Crisco T, Oxland T. Three-dimensional movements of the whole lumbar spine. *J Biomech.* 1989;22:1103.
45. Schmoelz W, Huber JF, Nydegger T, Dipl-Ing CL, Wilke HJ. Dynamic stabilization of the lumbar spine and its effects on adjacent segments: an in vitro experiment. *J Spinal Disord Tech.* 2003;16:418–23.
46. Panjabi MM, Oxland TR, Yamamoto I, Crisco JJ. Mechanical behavior of the human lumbar and lumbosacral spine as shown by three-dimensional load-displacement curves. *J Bone Jt Surg Am.* 1994;76:413–24.
47. Erbulut DU, Zafarparandeh I, Hassan CR, Lazoglu I, Ozer AF. Determination of the biomechanical effect of an interspinous process device on implanted and adjacent lumbar spinal segments using a hybrid testing protocol: a finite-element study. *J Neurosurg Spine.* 2015;23:200–8.
48. Chen CS, Cheng CK, Liu CL, Lo WH. Stress analysis of the disc adjacent to interbody fusion in lumbar spine. *Med Eng Phys.* 2001;23:485–93.
49. Devroey C, Jonkers I, de Becker A, Lenaerts G, Spaepen A. Evaluation of the effect of backpack load and position during standing and walking using biomechanical, physiological and subjective measures. *Ergonomics.* 2007;50: 728–42.
50. Liu T, Khalaf K, Adeeb S, El-Rich M. Numerical investigation of intra-abdominal pressure effects on spinal loads and load-sharing in forward flexion. *Front Bioeng Biotechnol.* 2019;7:1–12.
51. Wettenschwiler PD, Lorenzetti S, Ferguson SJ, Stämpfli R, Aiyangar AK, Rossi RM, et al. Loading of the lumbar spine during backpack carriage. *Comput Methods Biomech Biomed Engin.* 2017;20:558–65.
52. Peng YX, Zheng ZY, Wang Md WG, Liu L, Chen MF, Xu Md HT, et al. Relationship between the location of ligamentum flavum hypertrophy and its stress in finite element analysis. *Orthop Surg.* 2020;12(3):974–82.
53. Ashton-Miller JA, Schmatz C, Schultz AB. Lumbar disc degeneration: correlation with age, sex, and spine level in 600 autopsy specimens. *Spine.* 1988;13:173–8.
54. Sun K, Liang L, Yin H, Yu J, Feng M, Zhan J, et al. Manipulation for treatment of degenerative lumbar spondylolisthesis: a protocol of systematic review and meta-analysis. *Medicine.* 2019;98:4–7.
55. Li K, Zhang SJ, Du CF, Zhao JZ, Liu Q, Zhang CQ, et al. Effect of strain rates on failure of mechanical properties of lumbar intervertebral disc under flexion. *Orthop Surg.* 2020;12(6):1980–9.